Advanced Steel Construction – Vol. 16 No. 3 (2020) 216–222
DOI:10.18057/IJASC.2020.16.3.3

EXPERIMENTAL AND THEORETICAL STUDY ON THE BEHAVIOR OF THE LAMINATED ACTION OF STEEL-CONCRETE COMPOSITE BEAM IN NEGATIVE BENDING MOMENT REGION

Xian Liang, Shu-Jin Duan *, Yuan-Yuan Wang and Yan-Qing Zhang

Research Institute of Structural Engineering, Shijiazhuang Tiedao University,Shijiazhuang, China
**(Corresponding author: E-mail: duanshujin@stdu.edu.cn)*

A B S T R A C T

A new type of steel-concrete composite-laminated action beams (CLB) is developed to improve the crack resistance of top concrete slabs. It is an improved version of double steel-concrete composite beams (DCB), in which the shear stress between top concrete slab and upper steel flange is released by the uplift-restricted and slip-permitted connectors (URSP). To investigate the static mechanical behavior of CLBs in the negative moment region, an experimental test on two CLB specimens and one DCB specimen was carried out, and the theoretical study on the distribution equation of interface slip, the calculation formulas of sectional bending stiffness and ultimate bending moments was conducted. The results show that although the flexural bearing capacity of CLB is slightly lower than that of DCB, the crack resistance was markedly better than that of DCB. The slips and ultimate bending moments predicted with the simplified formulas are good in agreement with tests results.

A R T I C L E H I S T O R Y

Received: 25 September 2019
Revised: 4 May 2020
Accepted: 30 May 2020

K E Y W O R D S

Composite-laminated action beam;
Cracking resistance;
Slippage; Bearing capacity;
Double composite beam;
Experimental study

1. Introduction

Traditional steel and concrete composite beams have been widely used in civil engineering in the past several decades because of their low weight, low cost, and the performances of the full use of the two materials. However, in the negative bending moment region of continuous beams, especially the long-span continuous beams, concrete cracking and steel flange buckling always troubled engineers [1-3]. In order to alleviate the local yield of the pressed web and the bottom flange of the steel beam, the double composite beam (DCB) was proposed by Reiner [4], as shown in Fig. 1 (a). In DCBs, the bending stiffness and strength were enhanced and local buckling of the steel profile in the negative moment region was prevented by attaching a concrete slab to the bottom flange of the steel beam.

In order to study the behavior of DCB, extensive researches has been conducted. Steven et al. [5] introduced that the inclusion of the double composite action provided several beneficial features: steel consumption was saved, a “braced effect” let the steel stress reduction factor unnecessary; a compact section is reasonably achieved in the negative flexural region, and the redistribution of moments becomes favorable; the width of frame may be reduced due to the bracing of bottom flange of the girder by bottom slab. Experiment studys [6]showed that the DCB could prevent local buckling of steel profile, improve the ductility of structure, and enlarge crack widths but slow crack development to some extent. Duan et al. [7-10] investigated the mechanical properties of DCB in the negative moment region by conducting experimental, numerical and theoretical studies. It was concluded that the elastic ultimate load of the DCB was increased about 50% compared the traditional composite beam, and under the action of the same load, the addition of lower concrete slab greatly reduced the maximum crack width.

In the DCB, the bending stiffness of cross sections was greatly increased, and the steel beam yielding under compression was alleviated. However, the neutral axis of cross sections was moved down, so the cracking in the top concrete slab was severe still [6,8].

Concrete cracks will degrade the cross-section stiffness and reduce the suitability and durability of structures. To improve the crack resistance of top concrete slab effectively in the negative moment region, many investigations have been conducted. Experimental studies [11] found that cracks concentrated at the cast interface of joints between decks even in the negative moment region. The inelastic behavior of the negative moment region and the cracking characteristics of the composite beams were investigated in the reference [12-13]. Researchers began to look for new design methods, materials and techniques. The crack development pattern was summarized, and a formula for calculating the maximum crack width was also given [14-18].

In practical engineering, the application of prestressed is the most common and effective method to relieve the cracking of concrete slab [19-20]. However, the prestressed construction process is complicated; the efficiency is low; and the bending stiffness improvement in the negative bending moment region is very limited. Therefore, scholars began to seek new ways to relieve the concrete cracking. The variation of strength and stiffness properties of beams with various degrees of composite beam was investigated in the literature [21], and the influence of the degree of partial composite action on flexural behavior was assessed. Experimental studies [22] showed that the cracking of the top concrete slab could be relieved by reducing the number of shear connectors. Changing the arrangement of the shear connectors, the cracking bending moment of the top concrete slab can be improved, and the maximum width of cracks also can be reduced [23]. Based on the viewpoint of reducing the transmission of the shear stress while maintaining the consistent of the vertical displacement of the concrete slab and the steel beam, the uplift-restricted and slip-permitted (URSP) connector was proposed [24]. And the mechanical properties and slip performance of URSP connectors have been investigated by conducting experiment and theoretical analysis [25-26].

With the DCB and URSP connectors as the background, a composite-laminated action beam (CLB) applied in the negative bending moment region of continuous composite beams was proposed [27]. The construction of CLB is shown in Fig. 1(b), in which the connectors connecting the top concrete slab and the steel beam is URSP connectors. According to the research about CLBs applied in the practical engineering, the composite-laminated action can effectively improve the stiffness of the cross-section in the negative bending moment region of continuous composite beams, and adjust the internal force of structures, thereby improving the mechanical performance of structures [28-29].

In order to study the mechanical properties of the new structure—CLB, an experiment of negative moment region was conducted. Two CLB specimens and one DCB specimen with the same parameters were designed and tested for comparison. The theoretically study of CLB is also conducted. The formulas for calculating the ultimate flexural capacity, bending stiffness, and slip distribution of CLB were proposed.

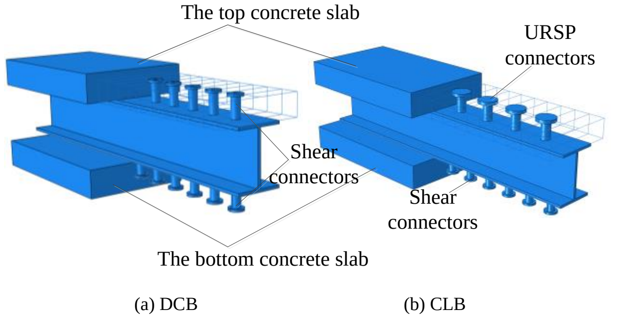

Fig. 1 Steel-concrete composite beam with different composition

2. Experimental studies

2.1. Specimens

As stated above, two CLBs (CLB1 and CLB2) and one DCB specimens were manufactured and tested. All these specimens had the same dimensions. Each specimen was 3.2 m long, and the net-span was 3.0 m with a 100-mm extent portion at each edge support. The main characteristics and nominal dimensions of test specimens are shown in Fig. 2(a), (b) and (c).

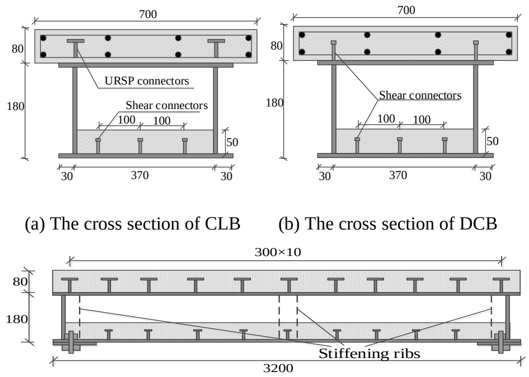

(a) The cross section of CLB (b) The cross section of DCB

(c) The arrangement of connectors

Fig. 2 Parameters of test beams (mm)

In the CLB, a laminated interface was formed between the top concrete slab and the steel beam using the URSP connectors, so the cross section was divided into top and bottom beams along the laminated interface.

The top concrete slab was 80 mm thick and 700 mm wide, and the bottom concrete slab was 50 mm thick and 362 mm wide. In the top concrete slab, 8 longitudinal rebars with 12mm diameter in two layers, and transverse bars with 6mm diameter and 100mm spacing were reinforced.

The steel beam was welded by 8-mm-thick SS400 steel plates. It was 180 mm high and 430 mm wide. Stiffening ribs were established at the support and loading sections, as shown in Fig. 2. The diameter and height of the connectors were 13 mm and 50 mm respectively. Fig.3 shows the construction of the URSP and shear connectors.

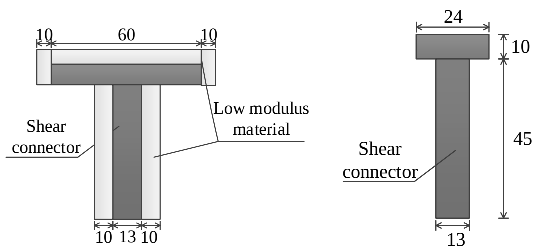

(a)URSP connector (b)Shear connector

Fig. 3 The Construction of connectors

2.2. Material Properties

The concrete material properties of specimens were tested on test day. The uniaxial compressive and tensile strengths were obtained based on 150-mm^3 cubic specimens. The mean yield strength, ultimate strength, and Young's modulus of welded steel plates and reinforcing steel bars were tested. The results are given in Table 1.

2.3. Test Setup and Loading Instrumentation

To simulate the stress state in the negative moment region, two ends of each specimen were connected to the ground though military piers. A reverse vertical load was applied to the mid-span by a hydraulic jack. The setup and test details are shown in Fig. 4.

In the negative moment region, as shown in Fig. 5, strain gauges were mounted on several critical cross sections of specimens and steel reinforcing bars to derive the sectional strain distribution. These critical cross sections were mainly positioned at 1/4 and 3/4 of the span, as well as at the cross sections 200 mm and 400 mm away from the mid-span. Fig.5 demonstrates the distribution of strain gauges mounted in the cross section of the 1/4 span, and strain gauges in other critical cross sections were mounted in this manner.

Table 1
Mechanical properties of materials (MPa)

Concrete	f_c	f_t	E_c	Steel	f_y	f_u	E_s
Top concrete	27.8	3.12	3.25×10^4	Steel plate	378.1	484.5	2×10^5
				Steel reinforce bar Φ12	456.7	615.0	2.06×10^5
Bottom concrete	29.0	3.20	3.25×10^4	Steel reinforce bar Φ6	300.5	420.2	2.06×10^5

Note: f_c and f_t are the compressive and tensile strength of concrete respectively; f_y and f_u are the yield and ultimate strength of steel respectively; E_c and E_s are the Young's modulus of concrete and steel.

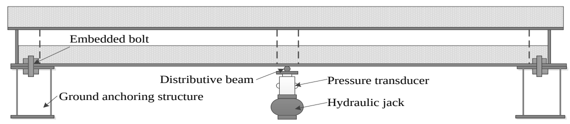

Fig. 4 Setup of test specimen

The vertical displacements was measured by displacement meters(LVDT) and the interlayer slip was measured by several dial indicators in the longitudinal direction. The locations of the LVDTs and the dial indicators were showed in Fig. 5.

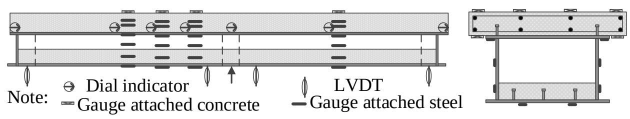

Fig. 5 Arrangement of measuring points

During testing, the cracking process, including position, direction and width, were also recorded in detail. The crack width was measured at several key load steps by an intelligent crack observation device (F61 Intelligent crack width tester).

In order to remove the gaps between specimens and loading machine, all specimens were preloaded before the formal test. After that, monotonic loading was applied by the hydraulic jack. The loading was controlled by force. The load increment imposed was 10 kN for each stage at the initiation of the test; when the cracking load was approached, the load increment was reduced to 5 kN to observe the development of cracks. After concrete cracking, the load increment was improved to 20 kN, and when the load reached approximately 80% of the expected ultimate bearing capacity, the load increment for each stage was reduced to 10 kN until the specimens failed. The loading was held constant for 2 min when reaching the default during each stage.

3. Test results analysis

There were three distinct stages in a typical composite beam failure process. Stage I was the stage before concrete cracking, and the materials behaved mainly elastically in this stage. Stage II corresponded to the stage in which concrete had been cracked but the steel profile had not yet yielded. In this stage, the bending stiffness of beams was weakened clearly, and non-linearity started to show in the load-deformation relationship curves. Generally, the ending of this stage is considered as the elastic limit. A composite beam in service is usually in stage II. Stage III started with the yielding of steel profile edge and ended with the failure of beams. In this stage, the bending stiffness of beams is weakened further.

At the end of stage I, cracks first appeared on the top surface of concrete slab at the mid-span position, and the initial tiny cracks did not change the bending stiffness of specimens obviously. In stage II, the steel beam was in the elasticity stage: the nonabsolutely linear behaviors and the stiffness declines were exhibited. The ultimate bearing capacity in this stage was approximately 0.8 P_u (where P_u was the ultimate bearing capacity). In stage III, the deformation increased rapidly, and the bearing capacity began to decline at the end of this stage. Fig. 6 shows the failure states of CLB1, which exhibited "flexural failure"

3.1. Load-deflection relation

The load-deflection curves of three specimens are shown in Fig. 7. It reflects the relationship between load and deflection at the position of 200 mm distance from the mid-span.The duration time of stage I was very short in the action of negative bending moment for both CLB and DCB. When the load reached 35.7 kN, the initial crack appeared in DCB. The corresponding cracking loads of CLB1 and CLB2 were 70.71 kN and 69.43 kN respectively. The cracking loads of the two CLBs were approximately two times that of DCB.

(a) Bending state (b) Cracking state

Fig. 6 Failure states of the CLB1

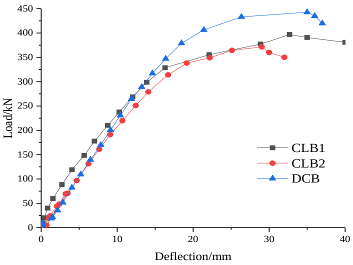

Fig. 7 Load-deflection relationship curves

From load-deflection curves, the non - linearity is obvious of both CLBs and DCB. The ultimate bearing capacity of DCB was greater than those of CLBs, but the elastic ultimate bearing capacity of CLBs were basically equivalent to DCB.

3.2. Cracking

In this and the following sections, take CLB1 and the DCB as examples for discussion because the distribution and development of cracks, strain, and stress of the CLB2 were similar to those of CLB1. Fig. 8 shows the crack development at critical loads in stages I and II. The development curves of the maximum crack width as the load increased were showed in Fig. 9. The shapes of the cracks reflect that the cracks were induced by a negative bending moment. Moreover, the symmetric distribution of crack around mid-span indicates that the loads were exerted symmetrically and equivalently around the mid-spans of the specimens.

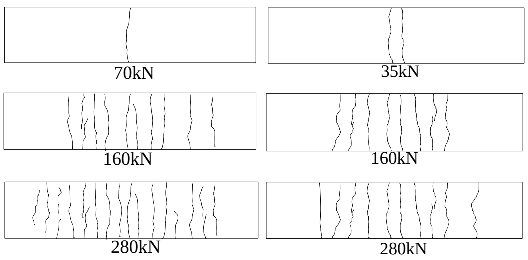

(a) CLB1 (b) DCB

Fig. 8 Crack formation and distribution

Due to different connector configurations, CLB1 exhibited flexural cracks, while DCB exhibited tensile cracks. More cracks were detected in CLB1 but the maximum crack width in CLB1 was always smaller than that of DCB.

It can be concluded that the crack resistance of the concrete slab could be greatly improved with the laminated action compared to the composite action The spacing between the main transverse cracks was almost 100 mm in CLB1 and 150 mm in DCB, which was close to the spacing of stirrups in corresponding specimens.

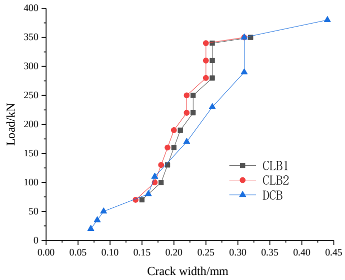

Fig. 9 Curves of load-maximum crack width

3.3. Distribution of strain and plastic neutral axis

The mechanical properties of composite beams were depend largely on the position of neutral axis in cross sections. The strain distribution along the cross-sectional height at the position of 200 mm away from the mid-span at different loading stages were showed in Fig. 10.

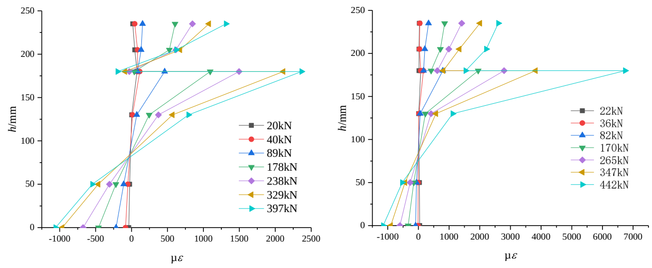

(a) Strain distributions in CLB1 (b) Strain distributions in DCB

Fig. 10 Sectional strain distributions

In Fig. 10(a), the slip occurred under a low load level in CLB1, and before that, the strain distribution along the section was linear and satisfied the assumption of a plane section. The top and bottom beams still worked together as a whole after slip occurred excepting for the change of neutral axis. In the middle stage of loading, the bottom of the top beam began to be compressed, and at the same time, two neutral axes appeared in the cross section. It is because the initial bond between top and bottom beams was damaged as load increasing. After that, the top and bottom beams in CLB1 were bent and deformed respectively around their own neutral axes under the premise of keeping the same vertical deformation. The strain distribution along the cross-sectional height of DCB is shown in Fig. 10(b). The difference from the strain distribution of CLB1 was that there was only one neutral axis during the entire loading process, indicating that the top and bottom beams were always a whole structure in the process of stress.

3.4. Relative slip

Measured the maximum slip—load curves were presented in Fig. 11. As shown in Fig. 11, the maximum slippages of CLB1 and CLB2 were approximately two times greater than that of DCB. The slippage distribution along the length of specimens CLB1 and DCB is presented in Fig. 12(a) and (b) respectively, where the horizontal axis *l* is the distance from the mid-span to the measured section. It indicates clearly from Fig. 12(a) and (b) that the slippage was distributed non-linearly along the longitudinal of specimens. This is because the slippage was extremely minor and affected by many factors such as stud weld quality, compaction rate of concrete, and eccentric loading, etc. The greatest slippages of CLB1 and DCB appeared at different positions. For CLB1, the greatest slippage was at the ends of specimen, but for DCB, it was at the position of 1/4 or 3/4 of specimen's span.

4. Analytical studies of the CLB

4.1. Sectional bending stiffness

Bending stiffness of a cross-section refers to the ability of a member to resist changes in its curved shape. It is the basis for analyzing the deflection and deformation of a structure under load and the ductility of the structure, and is also used in calculating the crack width of a concrete structural member. Therefore, the bending stiffness is very important for the structural mechanical performance analysis.

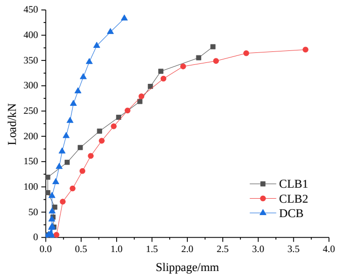

Fig. 11 Load-slippage relationship

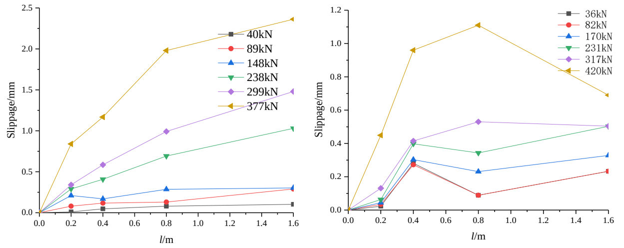

(a) CLB1 (b) DCB

Fig. 12 Load-slippage relationship

The cross-sectional bending stiffness calculation formulas of laminated beams without considering the friction effect have been given in the material mechanics [30]. However, before interface slip appears, the friction force in the rough interface will hinder the slippage and increase the bending stiffness of beams. Therefore, the calculation formulas of bending stiffness considering the action of friction will be obtained through the theoretical analysis in this section.

The micro-segment analysis model of CLB under the action of negative bending moment is shown in Fig. 13. B_1, E_1, A_1 and I_1 are the bending stiffness, elastic modulus, cross-sectional area and moment of inertia of the top beam, respectively, and the relevant parameters of the bottom beam are B_2, E_2, A_2 and I_2, respectively.

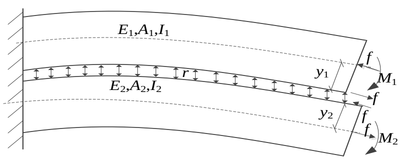

Fig. 13 Micro-segment analysis model

Under the action of the interface friction force f, the resistance bending moments M_{f1} and M_{f2} generated at the neutral axis positions of the top and bottom beams can be expressed as:

$$M_{fi} = fy_i \tag{1}$$

where i=1,2. The y_1 and y_2 are the distances from the neutral axis of top and bottom beams to the laminated interface.

The bending curvature ϕ_{fi} generated by the resistance bending moments to the top and bottom beams are:

$$\phi_{fi} = \frac{M_{fi}}{E_i I_i} \tag{2}$$

In CLB, the bending stiffness of bottom beam is greater than that of top beam, which results in $\phi_{f1}>\phi_{f2}$. As shown in Fig. 14, the top and bottom beams will separate under the resistance bending moment action. Under the action of URSP connectors, CLB can prevent the separation of top and bottom beams effectively, and keep the curvature of top and bottom beams consistent. Therefore, the smaller one of ϕ_{f1} and ϕ_{f2} is taken as the influence of the resistance bending moment on the bending curvature of cross-section.

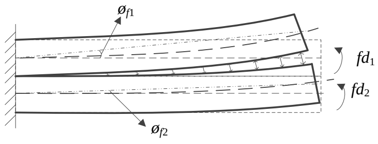

Fig. 14 Bending shape of CLB

The top and bottom beams' resistance strains ε_1 and ε_2 caused by the interfacial friction force f are:

$$\varepsilon_i = \frac{f}{E_i A_i} \tag{3}$$

The bending curvature caused by the resistance strain on the cross-section is ϕ_f', expressed as:

$$\phi_f' = \frac{\varepsilon_1 + \varepsilon_2}{y_1 + y_2} \tag{4}$$

Combining equations (3) and (4), the resistance curvature of cross section generated by friction resistance is ϕ:

$$\phi = \frac{f}{y_{sc}}\left(\frac{1}{E_1 A_1} + \frac{1}{E_2 A_2}\right) + \frac{fy_2}{E_2 I_2} \tag{5}$$

where the $y_{sc}=y_1+y_2$.

The additional bending stiffness K_f caused by the friction can be expressed as:

$$K_f = \frac{f}{y_{sc}}\left(\frac{1}{E_1 A_1} + \frac{1}{E_2 A_2}\right) + \frac{fy_2}{E_2 I_2} \tag{6}$$

The sectional bending stiffness in the negative bending moment region, B can be expressed as:

$$B = B_1 + B_2 + K_f \tag{7}$$

4.2. Calculation of ultimate flexural capacity

As shown in Fig. 15, there are two plastic neutral axes in CLB, the bending moment of CLB is the bending moment sum of top and bottom beam.

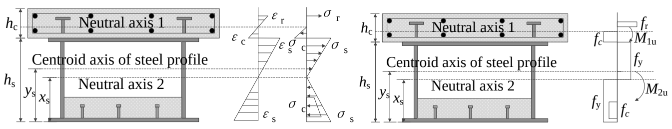

(a) Calculation model of M_e (b) Calculation model of M_u

Fig. 15 Calculation model of ultimate bending moment

A calculation model for ultimate flexural capacity was proposed based on the transformed section method and the simplified plastic theory. It is reasonable to assume that: (1) ignoring the tensile strength of concrete; (2) the cross section as a compact one, meaning that the steel profile would not lose stability under pressure before reaching the cross-sectional carrying capacity ; and (3) without considering the natural adhesion force of laminated interface.

The whole process of stress can be divided into three distinct stages [31], the stress and strain distribution along cross-section height at each stage are shown in Fig. 15.

(1) The stage before concrete cracking($M \le M_{cr}$)

The top reinforced concrete slab of CLB will crack under a small negative bending moment, and the cracking moment can be expressed as [32]:

$$M_{cr} = \frac{\gamma_m W_0 f_t}{n} \tag{8}$$

where the γ_m is the resistance coefficient of section, it is 5.5 for a rectangular concrete slab; W_0 is the cross-section resistance, $W_0=2I_1/h_c$, h_c is the height of top beam; f_t is the tensile strength of concrete; n is the coefficient of stiffness distribution, $n=B_1/(B_1+B_2)$.

(2) The stage of elasticity working($M_{cr} \le M \le M_y$)

After concrete cracking, the steel beam is still in the elastic working stage. In this stage, CLB is approximately in an elastic working stage. The neutral axis moves down with the increase of moment, the deflection and rotation increase fast.

$$M_y = M_{1y} + M_{2y} \tag{9}$$

where M_{1y} and M_{2y} are the elasticity ultimate bending moments of top and bottom beams, respectively.

$$M_{1y} = A_r f_r \left(\frac{h_c}{2} - a - \frac{d}{2} \right) + f_c b_c \frac{h_c^{\ 2}}{8} \tag{10}$$

$$M_{2y} = \frac{f_y I_2}{h_s - x} \tag{11}$$

where A_r is the area of reinforcing steel bar, b_c, h_c is the width and height of top beam respectively, h_s is the height of steel beam, d is the diameter of reinforcing steel bar, and a is the thickness of protective layer, f_r is the tensile strength of reinforcing steel bar.

(3) The stage of plasticity working ($M_y \le M \le M_u$)

When the tensile steel profile reaches yield strength f_y, the bending moment $M_y \approx (0.8 \sim 0.9) M_u$. The yield range of steel beam expands further with the increase of moment. Based on the theory of total plasticity, the ultimate moment M_{1u} of top beam and M_{2u} of bottom beam can be expressed as:

$$M_{1u} = a_1 f_c b_c \frac{x_c^{\ 2}}{2} + f_r \frac{A_r}{2}(x_c - a) + f_r \frac{A_r}{2}(h_c - x_c - a) \tag{12}$$

$$M_{2u} = W_x f_y + a_1 f_c b_{c2} h_{c2} (x_s + \frac{y_w}{2} - t_{f2} - \frac{h_{c2}}{2}) \tag{13}$$

where x_c is the thickness of the compressed concrete in the top beam, W_x is the cross-sectional bending coefficient of steel profile, b_{c2} and h_{c2} are the width and height of bottom concrete slab respectively, x_s and y_w are shown in Fig. 15(b).

4.3. Slippage distribution analysis

The bending stiffness is effected by the friction force, and the friction action will also affect the structural slippage. In this section, the theoretical analysis on the interface slip of simply supported CLB under the uniform and the reverse concentrated load is carried out to obtain the slip distribution equations along the beam's longitudinal.

Considering the symmetry of structure and the slippage distribution, analysis is conducted by taking the mid-span as the coordinate origin, and the range of x>0 as the analysis object (Fig. 16).

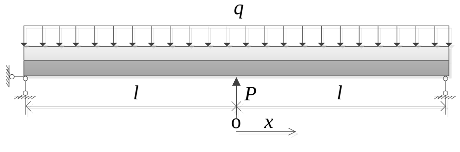

Fig. 16 Schematic diagram of structural analysis

4.3.1. Slip under uniform load

The micro-segment deformation model for negative bending moment of CLB under uniform load is shown in Fig. 17. In Fig. 17, T_1 and T_2 are the tensile forces of top and bottom beams, respectively; V_1 and V_2 are the shear forces of top and bottom beams, respectively; and r is the pressing force on laminated interface.

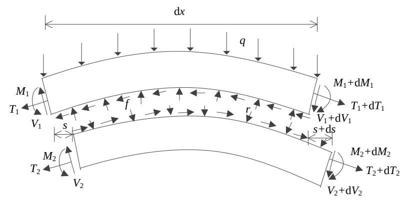

Fig. 17 Micro-segment deformation model under uniform load

The friction f existing on the laminated interface can be expressed as:

$$f = \mu r \tag{14}$$

where μ is the coefficient of friction.

The distribution of load is determined according to the bending stiffness of top and bottom beams [33-34], and the pressing force between the laminated interfaces is:

$$r = \frac{qE_2 I_2}{E_1 I_1 + E_2 I_2} \tag{15}$$

The bending moments on the left side of top and bottom beam units are taken and sorted out respectively:

$$-\frac{dM_1}{dx} + (V_1 + dV_1) + (q - r)\frac{dx}{2} + \mu r y_1 = 0 \tag{16-1}$$

$$-\frac{dM_2}{dx} + (V_2 + dV_2) + r\frac{dx}{2} + \mu r y_2 = 0 \tag{16-2}$$

Assuming that the distance of the micro-segment to the right support to be a(a=l-x):

$$V_1 + dV_1 + V_2 + dV_2 = -qx \tag{17}$$

According to the assumption (1):

$$\phi = \frac{M_1}{E_1 I_1} = \frac{M_2}{E_2 I_2} \tag{18}$$

where ϕ is the curvature of cross-section, as well as the top and bottom beams.

The compressive strain at the bottom of the top beam and the tensile strain at the top of the bottom beam are:

$$\varepsilon_c = \phi y_1 - \frac{T_1}{E_1 A_1} \tag{19-1}$$

$$\varepsilon_t = \phi y_2 + \frac{T_2}{E_2 A_2} \tag{19-2}$$

Combining the above formulas, there is:

$$\frac{d\phi}{dx} = \frac{\mu r y_{sc} - qx}{EI} \tag{20}$$

where $EI=E_1I_1+E_2I_2$.

The expression of the first derivative of simply supported CLB slip strain is:

$$\varepsilon_s' = \frac{\mu r y_{sc} - qx}{EI} y_{sc} + \mu r\left(\frac{1}{E_1A_1} + \frac{1}{E_2A_2}\right) \tag{21}$$

The boundary conditions of slip and slip strain of simply supported CLB are:

$$\begin{cases} \varepsilon_s\big|_{x=l} = 0 \\ s\big|_{x=0} = 0 \end{cases} \tag{22}$$

The slip distribution equation of laminated interface under uniform load can be expressed as:

$$s = \frac{\frac{\mu r y_{sc} x(x-2l)}{2} - \frac{qx(x^2-3l^2)}{6}}{EI} y_{sc} + \mu r x(x-2l)\left(\frac{1}{2E_1A_1} + \frac{1}{2E_2A_2}\right) \tag{23}$$

4.3.2. Slip under concentrated load

Similar to the derivation under the uniform load, the slip distribution equation of laminated interface under concentrated load can be obtained:

$$s = \frac{P}{2EI} y_{sc}\left(\frac{x^2}{2} - xl\right) \tag{24}$$

where P is the concentrated load.

5. Comparisons

5.1. Slip comparison

In the experiment, the friction coefficient μ between the laminated interface was not measured. According to the relevant research [35], μ=0.7 was adopted to calculate the slip distribution. Theoretical predictions and experimental responses of CLB1 were shown in Fig. 18, the "*T*" represents theoretical predictions and the "*M*" represents measured experimental responses.

From Fig. 18, it can be seen that when the load is 60kN, the measured results are only about half of the analysis results, mainly due to the initial bonding between the top and bottom beam is still strong during the initial loading. As the load increasing, the measured values are about 10% smaller than the analytical values, which may still result from the interfacial adhesion or frictional force. By comparing the slip test results with the analysis results, it can be concluded that the slip distribution equations (23) and (24) considering the interfacial friction force is effective for analyzing the slip distribution of CLB.

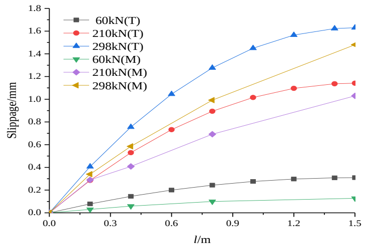

Fig. 18 Comparison of slip distribution curves

5.2. Ultimate flexural capacity comparison

The critical bending moments obtained from tests and predicted by theoretical analysis are tabulated in Table 2. It can be found that the Eqs. (6)-(11) and the calculation formulas in reference [7] can predict the critical bending moments of CLB and DCB well.

6. Conclusions

Experimental and analytical investigation on the mechanical behaviors of the laminated action steel-concrete composite beam has been conducted in this paper. The mechanical properties including development of cracks, slippage, ultimate bearing capacity of CLB and DCB were analyzed and compared. On the basis of theoretical analysis, the calculate formulas for bending stiffness of cross-section were given. Under negative bending moment, the slip distribution equations considering frictional force of simply supported CLB were conducted. The calculate formulas for ultimate bending carrying capacity were obtained. And the theoretical predictions and experimental responses were good agreement. The following conclusions may be drawn from the present study:

• The static failure mode of the CLB in the negative bending moment region is flexural failure, similar to that of the DCB. In the inelastic stage after concrete cracking, the ultimate bending capacity of CLB is almost equivalent to that of DCB.

• Concerning the cracks development of top concrete slab, it can be deduced that CLB exhibit flexural cracks, while DCB exhibit tensile cracks. Comparing with DCB, the cracking moment of CLB is nearly doubled, and the maximum crack width is reduced by about 50%. .

• The slip distribution formulas which are developed by considering the interfacial friction force are effective for analyzing the slip distribution of CLB. And the formulas obtained by theoretical analysis can predict the flexural bearing capacity of CLB well.

Table 1

Experimental and Analytical Results of Critical Bending Moments of Specimens

Limit state	CLB			DCB		
	Eqs. （kN・m）	Measured (kN・m）	Eqs. to measured	Eqs. （kN・m）	Measured (kN・m）	Eqs. to measured
Cracking bending moment	54.7	53.0	1.03	30.2	26.8	1.13
		52.1	1.05			
Elastic limit bending moment	239.5	246.5	0.97	269.7	260.4	1.04
		235.5	1.02			
Plastic limit bending moment	291.9	297.6	0.98	318.6	332.0	0.96
		278.5	1.04			

Acknowledgments

The work is supported by key project of Natural Science Foundation of Hebei Education Department, China (Contact No. ZD2018025) and the Shijiazhuang Tiedao University's Graduate Innovation Fund Project, China(No.YC 2018001)

References

[1] Fan, J.S., Gou, S.K., Ding, R., et al., "Experimental and analytical research on the flexural behaviour of steel ECC composite beams under negative bending moments", Engineering Structures, 210, 2019.

[2] Wang, Y., Li, T., "Numerical analysis of forces in negative bending region of steel-concrete composite beams". Sensors & Transducers, 168(4), 2014.

[3] Śledziewski Krzysztof,Górecki Marcin. "Finite element analysis of the stability of a sinusoidal web in steel and composite steel-concrete girders", Materials (Basel, Switzerland), 13(5), 2020.

[4] Reiner, S., "Bridges with double composite action", Structural Engineering International, 6(1), 32-36, 1996.

[5] Steven L. Stroh, Rajan Sen, "Steel bridges with double-composite action", Transportation Research Record, 1696, 299-309, 2000.

[6] Xu, C., Su, Q.T., Wu, C., Sugiura, K., "Experimental study on double composite action in the negative moment region of two-span continuous composite box girder", J. Constr. Steel Res, 67(10), 1636-1648, 2011.

[7] Duan, S.J., Huo, J.H., Zhou, Q.D., "Research on calculation method of ultimate bearing capacity of double steel-concrete composite beams", Journal of Shijiazhuang Railway

Institute (Natural Science Edition), (04), 1-5, 2007.
[8] Duan, S.J., Niu, R.M., Wang, W.C., et al., “Study on crack expansion mechanism and crack width of the double composite continuous beam”, Journal of the China Railway Society, 34(12), 96-101, 2012.
[9] Duan, S.J., Zhou, Q.D., Wang, H.L., et al., “Experimental study on bearing capacity of the double composite continuous beam”, Journal of Railway Science and Engineerin, (05), 12-17, 2008.
[10] Duan, S.J., Shao, X.H., Niu, R.M., et al., “Experimental study on interface slip of the steel-concrete double composite continuous beam”, Highway Traffic Science and Technolog, 26(07), 95-99, 2009.
[11] Ryu Hyung-Keun, Kim Young-Jin, Chang Sung-Pil., “Crack control of a continuous composite two-girder bridge with prefabricated slabs under static and fatigue loads”, Eng Struct, 29(6), 851-864, 2007.
[12] Chang-Su Shim, Hyung-Keun Ryu, Chul-Hun Chung, et al., “Inelastic behavior of a continuous composite box girder bridge with prefabricated slabs”, Composite Construction in Steel and Concrete V, Proceedings of the 5th International Conference, (02), 57-66, ASCE, July, 2006.
[13] He, J., Liu, Y.Q., Chen, A.R., et al., “Experimental study on inelastic mechanical behaviour of composite girders under hogging moment”, J. Constr. Steel Res., 66(1), 37-52, 2010.
[14] Dong, Y.Y., Xu, Y., “Research on anti-cracking design method of steel-concrete composite beams in negative moment zone”, Proceedings of 2019 International Conference on Virtual Reality and Intelligent Systems (ICVRIS 2019), Volume II, 143-146, 2019.
[15] L. K. Varshney, K. A. Patel, Sandeep Chaudhary, et al., “An efficient and novel strategy for control of cracking, creep and shrinkage effects in steel-concrete composite beams”, Structural Engineering and Mechanics, 70(6), 751-763, 2019.
[16] Nie, J.G., “Application of steel-concrete composite structure in ocean engineering”, Steel Construction, 35(1), 20-33, 2020.
[17] Ding, Y., Dai, X.M., Yan. J.B., “Development and behaviors of slip-released novel connectors in steel-concrete composite structures”, Advanced Steel Construction, 15(1), 30-36, 2019.
[18] Zhang, Y.L., “Experimental and theoretical study on the mechanical properties and cracking control of steel-concrete composite beams in negative bending moment region”, Ph.D. Dissertation, Beijing Jiaotong University, 2009.
[19] Wang, Y.H., Yu, J., Liu, J.P., et al., “Experimental study on assembled monolithic steel-prestressed concrete composite beam in negative moment”, Journal of Constructional Steel Research, 167, 2020.
[20] Chen, S.M., Wang, X.D., Jia, Y.L., “A comparative study of continuous steel-concrete composite beams prestressed with external tendons: experimental investigation”, J. Constr. Steel Res., 65(7), 1480-1489, 2009.
[21] Eray Baran,Cem Topkaya., “Behavior of steel–concrete partially composite beams with channel type shear connectors”, Journal of Constructional Steel Research, 97, 2014.
[22] Nie, J.G., Wei, J., “The actual performance of shear connector in steel-concrete composite beam”, Journal of Zhengzhou Institute of Technology, 04, 43-47, 1991.
[23] Liu, W.H., Chang, D.B., “Experiment study on the crack resistance of composite beams”, Journal of Jilin Architectural and Civil Engineering, 03, 1-3, 2008.
[24] Nie, J.G., Tao, M.X., Nie, X., et al., “New technique and application of uplift- restricted and slip-permitted connection”, China Civil Engineering Journal, (04), 7-14, 58, 2015.
[25] Nie, J.G., Li, Y.X., Tao, M.X., et al., “Resistance test of new type－uplift-restricted and slip-permitted connector”, China Journal of Highway and Transport, 27(04), 38-45, 2014.
[26] Nie, J.G., Ma, Y., “Experimental study on the resistance performance of uplift-restricted and slip-permitted studs connectors”, Special Structural Periodicals, 32(03), 6-12, 2015.
[27] Duan, S.J., Niu, R.M., An, R.M., et al., “Steel-concrete composite-laminated beam”, ZL 2016 2 1090805. 0, 2017.04.19. Chinese Patent.
[28] Nie, J.G., Tao, M.X., Wu, L.L., et al., “New progress in the study of steel-concrete composite bridge”, China Civil Engineering Journal, 45(06), 110-122, 2012.
[29] Nie J G, Wang J J, Guo S K, et al. “Technological development and engineering application of novel steel-concrete composite structure”, Frontiers of Structural and Civil Engineering. 2019, Vol.13 (1), pp.1-14
[30] Sun, X.F., Fang, X.S., Guan, L.T., “Material mechanics 1”, Beijing: Higher Education Press, 2009.
[31] Guo, Z.H., “Principles of reinforced concrete(3nd)”, Beijing: Tsinghua University Press, 2013.
[32] GB50010(2010), Code for Design of Concrete Structures, China Architecture & Building Press, Beijing, China, 2010.
[33] Shu, X.P., “Study on contact pressure of beams considering friction[J]. Mechanics and Practice”, 13(05), 23-26, 1991.
[34] Luo, K.B., “Analysis of contact pressure between laminated beams considering shear deformation”, Mechanics and Practice, 9(02), 34-38, 1987.
[35] Su, Q.T., Du, X., L, C.X. and Jiang, X., “Basic physical parameter test of the steel and concrete interface”, Journal of Tongji University(Natural science), 44(04), 499-506, 2016.